NASA TECHNICAL NOTE

NASA TN D-2353

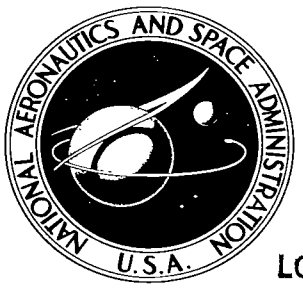

NASA TN D-2353

BUCKLING OF THE ECHO A-12 PASSIVE COMMUNICATIONS SATELLITE

by Wilbur B. Fichter, Harvey G. McComb, Jr., and Robert W. Leonard

Langley Research Center
Langley Station, Hampton, Va.

NATIONAL AERONAUTICS AND SPACE ADMINISTRATION • WASHINGTON, D. C. • JULY 1964

BUCKLING OF THE ECHO A-12 PASSIVE COMMUNICATIONS SATELLITE

By Wilbur B. Fichter, Harvey G. McComb, Jr.,
and Robert W. Leonard

Langley Research Center
Langley Station, Hampton, Va.

NATIONAL AERONAUTICS AND SPACE ADMINISTRATION

For sale by the Office of Technical Services, Department of Commerce,
Washington, D.C. 20230 -- Price $1.00

BUCKLING OF THE ECHO A-12 PASSIVE COMMUNICATIONS SATELLITE

By Wilbur B. Fichter, Harvey G. McComb, Jr.,
and Robert W. Leonard
Langley Research Center

SUMMARY

Experimental and theoretical studies have been conducted to obtain an estimate of the buckling strength of the Echo A-12 passive communications satellite. Results of experimental investigations of buckling of complete spherical shell specimens having very high radius-thickness ratios extend considerably the scope of existing experimental information. Experimental results are extrapolated by means of the classical linear theory to obtain estimates of the buckling strength of the full-scale satellite.

INTRODUCTION

The Echo A-12 passive communications satellite is an ultrathin-wall sphere intended to serve as a reflector for electromagnetic radiation. This spherical shell is 135 feet in diameter and fabricated of a three-layer laminate composed of plastic film (polyethylene terephthalate) with 1080 aluminum foil bonded on either side. (For a detailed discussion of the properties of this plastic film, see ref. 1.) The shell has 106 meridional gores bonded together in butt, single-strap splices. The straps are 1-inch-wide strips of the same three-layer laminate used in the gores and are bonded on the outside of the sphere. This lightweight satellite is to be folded compactly for the launch phase and then deployed by internal pressure after injection into orbit.

The shape of the inflatable satellite must remain essentially spherical so that its function as a reflector is not seriously impaired after loss of the internal pressure used to deploy it. Thus, large buckles induced by compressive stresses due to external pressure cannot be tolerated. Unfortunately, a direct prediction of the buckling strength of the full-scale satellite is beyond the present state of the art of shell analysis, due largely to numerous imperfections in shape which remain to some extent after deployment and at the time of exposure to the external loads of the operating environment.

However, a careful consideration of the buckling problem of the Echo A-12 sphere from the standpoint of current shell technology along with a reasonable extension of existing knowledge by means of tests on smaller but still very thin-wall spherical shells made from the same material as the Echo A-12 sphere should provide a sufficiently sound basis for estimating the buckling strength. Indeed, such a procedure must be relied upon, since meaningful buckling tests

of the full-scale sphere are virtually impossible in a 1g gravity environment. The purpose of this investigation is to provide a good estimate of the buckling strength of the Echo A-12 satellite. The basis of this estimate including results of buckling tests of small spheres made from the Echo A-12 laminate, is described.

This report includes an appendix by Robert W. Fralich of the Langley Research Center, which presents a linear analysis of the stresses in a spherical membrane acted upon by solar (or dynamic) pressure.

SYMBOLS

D	bending stiffness
E	Young's modulus
F	total unbalanced solar pressure or drag force
I	moment of inertia
K	extensional stiffness
L	length
ΔL	buckle half wave length
M	total mass of sphere
m	mass per unit area of sphere surface
$N = -\frac{pr}{2}$	
N_o	stress resultant due to initial inflation pressure
N_θ	circumferential stress resultant
N_ϕ	meridional stress resultant
p	pressure
Δp	differential pressure
r	radius of sphere
t	thickness
w	weight of a laminate strip per unit length

Y	intensity of tangential loading
Z	intensity of radial loading
θ,ϕ	angular coordinates
μ	Poisson's ratio

Subscripts:

Al2	Echo A-12
a	aluminum
cl	classical
f	plastic film
l	laminate
m	pertains to measured values
o	initial value
sol	solar

LOADS

Principal Loads

The principal sources of external load tending to buckle the Echo A-12 satellite are the direct pressure of photons from the sun (solar pressure) and the pressure exerted by impact with the molecules of the very thin atmosphere through which the sphere must orbit (denoted in this report by the term "dynamic pressure"). These two pressures are compared in figure 1 over a range of altitudes from 50 to 1,100 international nautical miles. The values shown are the stagnation pressures for assumed normal incidence and perfect reflectivity. For comparison, a curve of static pressure exerted by the atmospheric molecules is included in the figure. The solid portions of the curves are based on the 1959 ARDC Standard Atmosphere (ref. 2); the dashed portions of the curves are extrapolations (ref. 3). The atmosphere is known to expand and contract with increases and decreases in solar flare activity. Because the 1959 Standard Atmosphere is based on measurements made during a period of maximum solar activity, the static- and dynamic-pressure curves of figure 1 are believed to represent upper limits.

The solar pressure is constant in the vicinity of the earth at 1.3×10^{-9} psi and overshadows the dynamic pressure at the Echo A-12 injection altitude of 700 international nautical miles (fig. 1). If the satellite dips

into the atmosphere (as Echo I has been observed to do periodically), dynamic pressure increases and becomes greater than solar pressure below about 445 international nautical miles. This altitude is slightly below the observed low perigee of the Echo I satellite.

The actual distribution over the surface of the sphere of either solar or dynamic pressure is, of course, not uniform. In terms of the angular coordinate of any point on a meridian ϕ measured from the radius directed toward the pressure source (fig. 2), the normal pressure distribution due to either of these sources of pressure may be represented by $p \cos^2\phi$ over the windward half of the sphere and by zero over the leeward half. This unbalanced loading causes the sphere to accelerate through space, creating inertia forces on the skin which combine with the external pressure forces to cause stresses in the skin. The total combination of forces is in equilibrium but is distributed nonuniformly over the sphere and results in a nonuniform distribution of stresses in the skin. An approximation to these stresses has been obtained in appendix A by a linear stress analysis through use of membrane shell theory.

A uniform normal pressure p applied to all points of the sphere would yield everywhere

$$N_\phi = N_\theta = -\frac{pr}{2}$$

where N_ϕ and N_θ are, respectively, meridional and circumferential stress resultants (stresses integrated through the thickness) that are positive in tension and r is the radius of the sphere. The stresses determined in appendix A for solar or dynamic pressure loading are shown at various points on the sphere in figure 3 in terms of the uniform compressive stress resultant $N = -\frac{pr}{2}$. Maximum compressive stresses are seen to occur at the stagnation point and have the values

$$N_\phi = N_\theta = \frac{7}{8} N$$

Hence, from the standpoint of linear theory, an assumption that the incident solar or dynamic pressure is applied uniformly over the surface of the sphere is conservative. Also note that use of solar and dynamic pressures from figure 1 is conservative, since these curves are based on perfect reflectivity and perfect elastic rebound, neither of which conditions can be realized.

Other Loads

Other external loads which act on the Echo A-12 satellite are the pressure of radiation reflected from the earth and the pressure caused by micrometeoroid bombardment. Reflected radiation pressure ranges from zero in the earth's shadow to a maximum value which is much smaller than direct solar radiation pressure. Further, when the satellite is subjected to maximum reflected earth radiation, this radiation acts on the side of the sphere which is experiencing

no direct solar radiation. Hence, this additional load may be regarded as either negligible or as essentially accounted for if the direct radiation pressure is assumed to act on the entire surface. Estimates are sometimes given of the pressure due to micrometeoroid bombardment (for example, ref. 4 gives a maximum pressure of 3.9×10^{-13} psi); generally this pressure is thought to be negligible compared with solar radiation pressure, but the lack of knowledge of the micrometeoroid environment makes any estimate very unreliable.

The Echo A-12 satellite has two diametrically opposed radio beacons attached to the skin. Rotation of the satellite while in orbit would introduce concentrated loads at the radio beacons. Rotation, however, is to be avoided, if possible. Also, the gravity differential over the sphere may be of some significance because of the very low stiffness of the skin. In addition, temperature gradients in the satellite skin could have some effect on the overall performance. Distortions and stresses due to any of these effects are neglected in this investigation.

ESTIMATION OF BUCKLING STRENGTH OF ECHO A-12 SATELLITE

The classical linear buckling analysis of spherical shells under external pressure does not adequately predict experimental buckling results for two principal reasons: (1) the perfectly uniform conditions of loading and deformation prior to buckling assumed in the classical analysis are not realized in practice or in laboratory experiments, and (2) the analysis does not take into account imperfections in the shape or the condition of stress in the shell prior to loading.

The first difficulty could perhaps be overcome analytically for solar- or dynamic-pressure loading of the Echo A-12 satellite. The need is for, first, a nonlinear large-deflection analysis of the axisymmetric deformation and stress condition resulting from the applied nonuniform pressure and inertia loads and, second, an asymmetric linear analysis for the stability of this deformed state of stress and deflection. The nonlinear analysis is needed since the prebuckling deflections will be very large compared with the wall thickness. In effect these large deflections, occurring in the presence of the membrane stresses, act as initial imperfections to induce buckling at loads lower than the classical load in spite of the fact that the membrane stresses themselves are lower than they would be if the classical state of uniform loading were realized (see, for example, appendix A). Analyses of this type for shallow spherical caps under uniform pressure have recently been made (for example, ref. 5).

On the other hand, overcoming the second difficulty for the Echo A-12 sphere appears impossible, since the initial state of imperfection which exists in the sphere after handling, folding, inflation, and subsequent depressurization is impractical to define and describe analytically. These initial imperfections can be expected to be large, especially for low initial inflation pressures, and hence would be expected to have a significant effect on the buckling loads.

In view of this second difficulty, the performance of a difficult nonlinear analysis of a perfect sphere appears unwarranted. Rather, it seems more appropriate to use the simpler linear analysis as a basis for estimating the buckling strength of the full-scale configuration from experimental data obtained on smaller sphere specimens.

Linear Results

For the laminated three-layer Echo A-12 sphere, the classical linear buckling analysis leads to the following expression for the buckling pressure (see appendix B):

$$\Delta p_{cl} = \left(\frac{2}{r}\right)^2 \sqrt{DK}$$

where r is the sphere radius (810 in.) and D and K are the bending and extensional stiffnesses of the laminated skin as given by equations (B2) and (B1) in appendix B. Numerical values of the stiffness constants D and K are discussed in appendix C where consideration of nominal and measured values of thickness and modulus leads to a range of values of each, as follows:

$$D = (23.8 \text{ to } 51.5) \times 10^{-5} \text{ lb-in.}$$

$$K = 3{,}055 \text{ to } 4{,}143 \text{ lb/in.}$$

Use of these values of D and K yields the following range of values of the classical buckling pressure for the full-scale Echo A-12 sphere:

$$\left(\Delta p_{cl}\right)_{A12} = (52 \text{ to } 89) \times 10^{-7} \text{ psi}$$

Adjustment of Linear Results on Basis of Experiment

The two sources of experience which provide a basis for selecting a reduction factor to be applied to the classical result are the experimental data existing in the literature and new experiments conducted with specimens made from the Echo A-12 laminate.

Experimental data from literature.- Practically all the published data have been obtained on shallow spherical segments with radius-thickness ratios of about 1,000 and below, clamped around the periphery and loaded by uniform external pressure (refs. 6 to 11). These tests, in common with the full-scale satellite acted on by solar pressure or atmospheric drag, were all complicated by the presence of large prebuckling deformations and, in some instances, by moderately large initial imperfections. The measured buckling pressures ranged from 20 percent to 60 percent of the classical calculation. Only a few tests have been reported in the literature on anything approaching a complete sphere

(refs. 6, 11, and 12). These results were obtained on hemispheres and yielded buckling pressures from 25 percent to 67 percent of the classical value.

New experimental results.- To provide more suitable experience on which to base an estimate of the buckling load of the full-scale satellite, tests have been made on two sphere specimens constructed from the Echo A-12 laminate. These specimens were 30 inches and 12.5 feet in diameter with radius-thickness ratios of approximately 17,000 and 85,000, respectively. The tests, which represent a considerable extension of the available experimental data, are described in detail in appendix D.

The specimens were inflated from a folded condition (fig. 4) and prestressed with progressively higher values of internal pressure. After each prestressing inflation, the internal pressure was reduced to atmospheric pressure and then slowly reduced until buckling occurred.

Discussion of Results

Figure 5 is a plot, for both specimens, of $\left(\frac{\Delta p}{\Delta p_{cl}}\right)_m$ as a function of the prestress N_o, the stress resultant in the shell wall due to initial inflation pressure. The quantity $\left(\frac{\Delta p}{\Delta p_{cl}}\right)_m$ is the ratio of the measured buckling pressure to the classical buckling pressure computed from average values of laminate thicknesses obtained from measurements made on the specimens tested in the present investigation, a Young's modulus for the plastic film of 0.7×10^6 psi, and a Young's modulus for 1080 aluminum foil of 10^7 psi. For the smaller specimen, ratios of the measured buckling pressure to the classical value ranged from 0.044 to 0.110 and for the larger specimen, from 0.122 to 0.182. For both specimens a definite trend is observed: buckling pressures increased with increasing prestress level as initial imperfections are pulled out and then decreased somewhat at greater prestress levels. At the highest prestress levels some permanent deformation was detected in the gores of the specimens, and it is believed that this deformation induced the observed premature buckling.

The specimens were inflated with a mixture of air and helium in order to counteract the effect of gravity. As a result, a slight gradient in pressure differential across the wall existed from top to bottom of the specimen. Also, a small concentrated force existed at the supporting stem in spite of efforts to eliminate it by adjusting the ratio of helium to air in the inflating medium. These circumstances doubtless led to buckling pressures lower than those that would be obtained if the specimens were loaded by a uniform external pressure and if no support forces had been present. Corrections were made to the data to account for gradients in differential pressure.

As shown in figure 5, a considerable increase in buckling pressure is obtained by increasing the prestress level, which reduces the number and magnitude of random wrinkles and folding imperfections. These effects, however,

account for only a small part of the deviation of experimental buckling pressures from the classical buckling pressures. Also, these results suggest that further increases in initial inflation pressure would not result in large increases in buckling pressure even if the shell wall remained elastic. Thus, it would seem that effects other than the random wrinkles and folding pattern imperfections must play a large role in causing buckling to occur below the classical value. Possible other effects are overall distortions because of seam misalinement and discrepancies in gore dimensions, nonuniform loading due to the gradient in differential pressure with height and any concentrated force at the stem, and nonuniform properties of the shell-wall material.

Estimated Buckling Strength

Extrapolation of the buckling experience on the specimens to the full-scale satellite leads to the results also given in figure 5 for $\frac{(\Delta p)_{A12}}{(\Delta p)_{sol}}$ as a function of prestress from inflation, where $(\Delta p)_{sol}$ is the solar radiation pressure. The lowest of these estimated buckling loads was obtained from the series of tests on the 30-inch-diameter specimen and is 142 times the solar pressure. This loading corresponds to the dynamic pressure (fig. 1) at an altitude of about 215 international nautical miles. The series of tests on the 12.5-foot-diameter specimen gives considerably higher ratios of buckling pressure to solar pressure.

CONCLUSIONS

Results of experimental and theoretical studies of the buckling strength of the Echo A-12 passive communications satellite indicate the following conclusions:

1. External loads most likely to cause buckling are solar pressure and, at low altitudes, dynamic pressure.

2. Analytical prediction of buckling loads for the full-scale Echo A-12 satellite is beyond the present state of the art, largely because of the presence of severe and undefinable initial imperfections after depressurization. Thus, experience with buckling of smaller spheres must be utilized to estimate the buckling strength of the full-scale structure.

3. On the basis of tests of small spheres made from the Echo A-12 laminate, the buckling pressure for the full-scale satellite at the injection altitude of 700 international nautical miles is at least 142 times the solar radiation pressure, and the satellite should not buckle from dynamic pressure unless it dips below an altitude of about 215 international nautical miles.

4. The effects on the satellite of temperature gradients, rotation, and differential gravity, further complicated by the presence of concentrated masses, are less clear. These effects are not treated in this report.

Langley Research Center,
National Aeronautics and Space Administration,
Langley Station, Hampton, Va., March 23, 1964.

APPENDIX A

MEMBRANE STRESSES IN A SPHERE DUE TO SOLAR OR DYNAMIC PRESSURE

By Robert W. Fralich

In this appendix a linear analysis is given of the stresses in a spherical membrane acted upon by solar (or dynamic) pressure. The analysis begins with the membrane theory of symmetrically loaded shells of revolution presented on pages 434 (eq. (f)) and 435 (eq. (256)) of reference 13. Specializing these equations to a spherical membrane of radius r yields

$$\frac{d}{d\phi}\left(N_\phi \sin \phi\right) - N_\theta \cos \phi + Yr \sin \phi = 0 \tag{A1}$$

$$N_\phi + N_\theta + rZ = 0 \tag{A2}$$

where ϕ is the angular coordinate of any point on a meridian measured from the radius directed toward the pressure source (see fig. 2). The quantities Y and Z are the intensities of tangential and normal loading at each point and N_ϕ and N_θ are, respectively, the resulting meridional and circumferential stress resultants (the stresses integrated through the thickness).

The first task is the expression of the loading intensities Y and Z in terms of the pressure p exerted on a flat plate of unit area normal to the pressure source. These intensities have two parts: (1) the direct contribution of the impinging particles and (2) the inertia forces associated with the resulting acceleration of the sphere through space. The direct contribution is felt over only one-half the sphere and consists of the following normal forces only:

$$\left.\begin{aligned} Y_1 &= 0 \\ Z_1 &= p \cos^2\phi \end{aligned}\right\} \quad \left(0 \leqq \phi \leqq \frac{\pi}{2}\right)$$

$$Y_1 = Z_1 = 0 \qquad \left(\frac{\pi}{2} \leqq \phi \leqq \pi\right) \tag{A3}$$

where the subscript 1 refers to solar or dynamic pressure. The total force exerted on the sphere by the pressure p is then

$$F = \int_0^{2\pi} \int_0^{\pi/2} Z_1 r^2 \cos \phi \sin \phi \, d\phi \, d\theta \tag{A4}$$

where θ is the angular circumferential coordinate. Substituting equations (A3) into equation (A4) and integrating yields

$$F = \frac{1}{2} p\pi r^2 \tag{A5}$$

If m is the mass per unit area of the sphere surface, the total mass of the sphere is

$$M = 4\pi r^2 m \tag{A6}$$

The acceleration of the sphere is then given by

$$\frac{F}{M} = \frac{p}{8m} \tag{A7}$$

from which it follows that each unit area of the sphere surface is subjected to an inertial reaction force $-p/8$ directed opposite to the pressure p. This force has both tangential and normal components - namely,

$$\left.\begin{aligned} Y_2 &= -\frac{p}{8} \sin \phi \\ Z_2 &= -\frac{p}{8} \cos \phi \end{aligned}\right\} \qquad \left.\left(0 \leqq \phi \leqq \pi\right)\right\} \tag{A8}$$

where the subscript 2 refers to inertial loading. The total loading intensities are the sums of equations (A3) and (A8):

$$\left.\begin{aligned} Y &= -\frac{p}{8} \sin \phi \\ Z &= \frac{p}{8}\left(8 \cos^2\phi - \cos \phi\right) \end{aligned}\right\} \qquad \left.\left(0 \leqq \theta \leqq \frac{\pi}{2}\right)\right\} \tag{A9}$$

and

$$\left.\begin{aligned} Y &= -\frac{p}{8} \sin \phi \\ Z &= -\frac{p}{8} \cos \phi \end{aligned}\right\} \qquad \left.\left(\frac{\pi}{2} \leqq \phi \leqq \pi\right)\right\} \tag{A10}$$

Consider the region $0 \leqq \phi \leqq \frac{\pi}{2}$. Substitution of equations (A9) into equations (A1) and (A2) yields

$$\frac{d}{d\phi}(N_\phi \sin \phi) - N_\theta \cos \phi = \frac{pr}{8} \sin^2\phi \tag{A11}$$

$$N_\theta = \frac{pr}{8}(\cos \phi - 8 \cos^2\phi) - N_\phi \tag{A12}$$

Substituting equation (A12) into equation (A11) and expanding gives

$$\sin \phi \frac{dN_\phi}{d\phi} + 2N_\phi \cos \phi = \frac{pr}{8}(1 - 8 \cos^3\phi) \tag{A13}$$

If equation (A13) is multiplied through by $\sin \phi$, the left-hand side becomes a perfect differential; integrating and rearranging then yields

$$N_\phi = \frac{1}{\sin^2\phi}\left[C + \frac{pr}{8}(2 \cos^4\phi - \cos \phi)\right] \tag{A14}$$

where C is an arbitrary constant of integration. In order for N_ϕ to be finite at $\phi = 0$, the quantity in brackets must vanish; this condition yields $C = -\frac{pr}{8}$. Substituting for C in equation (A14) and further rearranging finally results in the following equation:

$$N_\phi = -\frac{pr}{2} + \frac{pr}{8}\left(\frac{3 + 2 \cos \phi - 2 \cos^2\phi - 2 \cos^3\phi}{1 + \cos \phi}\right) \qquad \left(0 \leqq \phi \leqq \frac{\pi}{2}\right) \tag{A15}$$

Substituting expression (A15) into equation (A12) then yields

$$N_\theta = -\frac{pr}{2} + \frac{pr}{8}\left(\frac{5 + 7 \cos \phi - 5 \cos^2\phi - 6 \cos^3\phi}{1 + \cos \phi}\right) \qquad \left(0 \leqq \phi \leqq \frac{\pi}{2}\right) \tag{A16}$$

The solution in the region $\frac{\pi}{2} \leqq \phi \leqq \pi$, where Y and Z are given by equations (A10), is precisely analogous to that just given (finiteness of N_ϕ at $\phi = \pi$ is the condition used to determine the constant of integration). The final results are as follows:

$$N_\phi = -\frac{pr}{2} + \frac{pr}{8}\left(\frac{3 - 4 \cos \phi}{1 - \cos \phi}\right) \qquad \left(\frac{\pi}{2} \leqq \phi \leqq \pi\right) \tag{A17}$$

$$N_\theta = -\frac{pr}{2} + \frac{pr}{8}\left(\frac{5 - 3\cos\phi - \cos^3\phi}{1 - \cos\phi}\right) \qquad \left(\frac{\pi}{2} \leqq \phi \leqq \pi\right) \qquad \text{(A18)}$$

If the solar (or dynamic) stagnation pressure were assumed to be uniformly applied normal to the entire surface of the sphere, the resulting compressive stresses would be $N_\phi = N_\theta = -\frac{pr}{2}$. Examination of equations (A15) to (A18) shows that the true compressive membrane stresses resulting from applied solar (or dynamic) pressure are everywhere smaller than the corresponding stresses which would be caused by a uniform pressure loading.

APPENDIX B

LINEAR BUCKLING ANALYSIS FOR A LAMINATED SPHERE

This appendix contains a generalization of the well-known linear buckling analysis for isotropic spherical shells under uniform external pressure (see, for example, ref. 14, pp. 512-518) to a three-layer laminated spherical shell like the Echo A-12.

The geometric assumptions of the classical linear theory are retained - that is, normals to the middle surface are assumed to remain straight and normal. Thus, it is assumed that a good bond exists between the layers of the laminate.

For the three-layer laminate, the extensional stiffness K and the bending stiffness D are given by

$$K = 2E_a t_a + E_m t_m \tag{B1}$$

$$D = \frac{E_a t_a (t_a + t_m)^2}{2(1 - \mu^2)} + 2\,\frac{E_a t_a^3}{12(1 - \mu^2)} + \frac{E_m t_m^3}{12(1 - \mu^2)} \tag{B2}$$

Note that D accounts for the bending stiffnesses of all individual layers as well as the displaced extensional stiffnesses of the outer layers. Hence, equation (B2) is valid for any combination of thicknesses and is not limited to relatively thin outer layers as is usual in sandwich shell theory.

The equilibrium equations (ref. 14, p. 513) for buckling of spherical shells apply equally to isotropic and laminated shells when expressed in terms of the stress and moment resultants. It follows that the buckling analysis presented in reference 14 (pp. 512-518) applies also to thin three-layer laminated shells if the extensional stiffness therein (Eh) is replaced by K as given in equation (B1) and the bending stiffness D is defined as in equation (B2). With these generalized forms of the extensional and bending stiffnesses kept distinct, the final result may be written

$$\Delta p_{cl} = \left(\frac{2}{r}\right)^2 \sqrt{DK} \tag{B3}$$

where Δp_{cl} is the calculated critical pressure for buckling and r is the radius of the sphere.

Equation (B3) is the analog of the well-known formula for isotropic spheres:

$$\Delta p_{cl} = \frac{2E_t^2}{r^2\sqrt{3(1 - \mu^2)}} \tag{B4}$$

Equation (B3), however, applies to any distribution of the material through the thickness with the proper definition of D and K and reduces to equation (B4) with the introduction of the isotropic stiffnesses:

$$\left.\begin{aligned} K &= Et \\ D &= \frac{Et^3}{12(1 - \mu^2)} \end{aligned}\right\} \tag{B5}$$

(Equations (B1) and (B2) apply only to the three-layer laminate.)

The buckle wave forms predicted by the linear theory are represented mathematically by Legendre polynomials of the first kind, $P_n(\cos \phi)$, where ϕ is the coordinate angle measured from the polar axis. For very thin-wall spheres n is very large, permitting an asymptotic approximation to be used except very near $\phi = 0$ or π (see ref. 15, p. 117):

$$P_n(\cos \phi) \sim \sqrt{\frac{2}{\pi n \sin \phi}} \sin n\phi \tag{B6}$$

From this formula it may be seen that the predicted wave forms have wave lengths which are very small compared with the circumference of the sphere. The value of n may be obtained from reference 14 in terms of the stiffnesses K and D for very thin spheres and corresponds to buckle half wave lengths on the surface given by

$$\Delta L = \pi r^{1/2}\left(\frac{D}{K}\right)^{1/4} \tag{B7}$$

APPENDIX C

STIFFNESS PROPERTIES OF THE ECHO A-12 LAMINATE

Thicknesses

Although the nominal thicknesses of the aluminum foil, plastic film, and laminate are given as

$$t_a = 0.00018 \text{ in.}$$

$$t_f = 0.00035 \text{ in.}$$

$$t_l = 0.00071 \text{ in.}$$

it appears, from measurements made in this investigation, that the nominal thicknesses can be taken to be the lower limits and that the following ranges of values can be ascribed to the thicknesses:

$$0.00018 \leqq t_a \leqq 0.00019$$

$$0.00035 \leqq t_f \leqq 0.00049$$

$$0.00071 \leqq t_l \leqq 0.00087$$

where, for simplicity, the thickness of the plastic film is assumed to include the thickness of the bonding agent. This assumption has a negligible effect on the calculated stiffnesses.

Material Properties

Aluminum-foil face sheet.- The aluminum-foil face sheet is composed of 1080 aluminum, which is 99.8 percent pure. No information on this material is given in the available literature, but for 1060 aluminum, which is 99.6 percent pure, the Young's modulus is given as 10^7 psi. The modulus for 1080 aluminum should not differ appreciably from the value given for 1060 aluminum; however, in order to obtain some information on the 1080 material, a series of stress-strain tests of the material was conducted with a tensile testing machine. One-inch-wide strips of the 1080 aluminum-foil face sheet were tested at low strain rates and at various levels of maximum stress from 0 to about 5,000 psi. Resulting measurements of Young's modulus were in the range (8 to 8.6) $\times$ 10^6 psi which seems unrealistically low; however, no reasonable explanation for these consistently low values is apparent.

Plastic film.- Although some investigators report a Young's modulus for the plastic film of (0.53 to 0.55) $\times 10^6$ psi, the results of other investigations (for example, ref. 16) including the present one give a value for the plastic film of about 0.7×10^6 psi. It appears that the use of $E_f = 0.5 \times 10^6$ psi to obtain a conservative value for the buckling strength would be appropriate.

Extensional Stiffness

Calculated.- The extensional stiffness of the laminate, given by equation (B1), is

$$K = 2E_a t_a + E_f t_f$$

To obtain a conservative value for K, the following values of the material properties may be used:

$E_a = 8 \times 10^6$ psi $\qquad t_a = 0.00018$ in.

$E_f = 0.5 \times 10^6$ psi $\qquad t_f = 0.00035$ in.

This procedure yields a value for K of 3,055 lb/in. When the highest measured values of the thicknesses, Young's modulus of the plastic film E_f, and what seems a reasonable estimate for the Young's modulus of 1080 aluminum $\left(E_a = 10^7 \text{ psi}\right)$ are used, the extensional stiffness K is 4,143 lb/in.

Measured.- Samples of the Echo A-12 laminate have been tested under cyclic loading to various levels of maximum stress from 0 to 6,000 psi (based on the aluminum area only). The results give the measured value for K of 3,710 lb/in.

Bending Stiffness

Calculated.- The bending stiffness of the laminate, given by equation (B2), is

$$D = \frac{E_a t_a (t_a + t_f)^2}{2(1 - \mu^2)} + 2\,\frac{E_a t_a^3}{12(1 - \mu^2)} + \frac{E_f t_f^3}{12(1 - \mu^2)}$$

where Poisson's ratio μ is assumed to be 1/3. (This assumption is reasonable for aluminum. Although Poisson's ratio is not well defined for the plastic film, it is not expected to differ appreciably from 1/3.) For a conservative value for the bending stiffness, the following values are used:

$E_a = 8 \times 10^6$ psi $\qquad t_a = 0.00018$ in.

$E_f = 0.5 \times 10^6$ psi $\qquad t_f = 0.00035$ in.

This procedure yields a value for D of 23.8×10^{-5} lb-in. A maximum value for the bending stiffness, using the previously disclosed maximum values for the material properties, is 51.5×10^{-5} lb-in.

Measured.- Measurement of the bending stiffness of thin films and laminates has been made possible by the solution of the "heavy elastica" problem given in reference 17. This problem concerns the bending from an initially horizontal position of a very flexible beam under its own weight. For a cantilever beam, the solution is presented in figure 5 of reference 17 in the form of a plot of the quantity $\frac{1}{L}\left(\frac{EI}{w}\right)^{1/3}$ as a function of the angle between the horizontal and a straight line connecting the root and tip of the deflected beam. The symbol EI denotes beam bending stiffness and w denotes beam weight per unit length. Plate bending stiffness D and beam bending stiffness EI are related by the following equation:

$$D = \frac{EI}{1 - \mu^2}$$

Measurements of the bending stiffness of the Echo A-12 laminate have been made by use of a simple pilot test device at the Langley Research Center along with the "heavy elastica" solution. Use of this device is in an exploratory stage, and results obtained for the Echo A-12 laminate are characterized by considerable scatter and some creep behavior. Until improved apparatus has been constructed and proper testing techniques evolved, the results must be considered approximate. They are in the range $24 \leqq D \times 10^5 \leqq 40$ which compares with the range $23.8 \leqq D \times 10^5 \leqq 51.5$ for calculated values.

APPENDIX D

BUCKLING EXPERIMENTS ON THIN-WALL SPHERE SPECIMENS

Experimental data are needed on which to base an estimate of the buckling strength of the Echo A-12 satellite. In order to provide more relevant data than appear in the literature, a series of buckling tests on two thin-wall sphere specimens has been made. These tests and their results are described in this appendix.

Specimens

The specimens tested (illustrated in fig. 6) were spherical shells 30 inches and 12.5 feet in diameter, fabricated of material similar to that used in the 135-foot-diameter Echo A-12 satellite. The material is a three-layer laminate composed of plastic film with an aluminum-foil face layer bonded on either side. The aluminum of the face layers is 99.8 percent pure and is designated as 1080 aluminum. The 30-inch- and 12.5-foot-diameter specimens had radius-thickness ratios, respectively, of about 17,000 and 85,000 compared with a ratio of about 1,000,000 for the full-scale Echo A-12 satellite.

The 30-inch- and 12.5-foot-diameter specimens had 17 and 23 meridional gores, respectively, bonded together in butt, single-strap splices. The straps were 1-inch-wide strips of the same three-layer laminate used in the gores and were bonded on the outside of the specimens. A small opening at one pole of each specimen provided access to the interior of the specimen for inflation and for control and measurement of internal pressure.

The full-scale Echo A-12 satellite is folded for the launch phase and deployed by inflation after injection into orbit. Depending on the magnitude of internal pressure used for deployment, the sphere may have various imperfections in shape after deployment. There may be many small wrinkles caused by routine handling and distributed at random over the surface. In addition, a regular pattern of creases may result from the folding (see fig. 4). Finally, some overall distortions may occur as a result of inaccuracies in gore dimensions or slight mismatching of the splices. All these imperfections were present in the test specimens.

Test Apparatus

30-inch-diameter specimen.- A copper T-fitting was inserted in the opening at one pole of the 30-inch-diameter specimen and supported on a table. To minimize the support forces on the specimen at the T-fitting, the specimen was floated in air by the use of helium mixed with air for a pressurizing medium. Pressurization and depressurization were accomplished through the side leg of the T-fitting and, for pressure measurement, a tube was inserted through the T-fitting a short distance into the specimen (fig. 6). This tube led to a

micromanometer with a pressure range of ±10 inches of water and a least count of 0.001 inch of water. Pressures were recorded manually and the data were supplemented with photographs.

12.5-foot-diameter specimen.- The 12.5-foot-diameter specimen was also floated in air by the use of a helium-air mixture for pressurization. Inserted into the opening at one pole was a fitting which accommodated tubes from the air and helium supplies and from the micromanometer (fig. 6). The fitting also accommodated a differential pressure indicator with a pressure range from 0 to 0.01 inch of water and a least count of 0.0001 inch of water. This sensitive differential pressure indicator was needed to measure the buckling pressures. The micromanometer was not sensitive enough to measure buckling pressures on this specimen and was used only to measure inflation pressures.

Since the support forces could be considerably greater for the large specimen than for the small specimen, the large specimen was mounted on scales which were counterweighted to balance the weight of the mounting fixture and inlet tubes. Then the proportion of air and helium was adjusted until the weight of the specimen was balanced by the buoyancy of the inflating gas. With this arrangement, the load at the support could be monitored at the scales and kept to a practical minimum throughout the series of tests.

Test Procedures

30-inch-diameter specimen.- The procedure for tests with the 30-inch-diameter specimen was to inflate the specimen to a desired internal pressure, to slowly reduce the pressure to zero, then to further reduce the pressure until buckling occurred. This procedure was repeated for progressively higher values of initial internal pressure from 0.034 to 10 inches of water, corresponding to skin stress resultants from 0.0092 to 2.7 lb/in.

When the specimen was inflated with a mixture of air and helium, fine pressure control was maintained by a test engineer by blowing into or drawing out on the supply tube as needed. Buckles were detected visually and by a sudden pressure change noticeable on the micromanometer. Pressures were recorded manually, and a series of photographs was taken during each test sequence.

12.5-foot-diameter specimen.- The procedure for tests with the 12.5-foot-diameter specimen was similar to that used for tests with the smaller specimen but differed in detail. The specimen was pressurized from air and helium supplies, while its buoyancy was monitored on the scale and kept to a practical minimum. Depressurization was accomplished with an ordinary tank-type vacuum cleaner through an outlet tube which was inserted through the support fitting and which extended about 2 feet into the specimen. A partial vacuum sufficient for depressurization was obtained by placing the exterior end of the outlet tube near the inlet of the vacuum cleaner. After a desired inflation pressure was attained, the pressure was slowly decreased until buckling occurred. As before, this procedure was repeated for progressively higher values of initial inflation pressure from 0.019 to 2.0 inches of water, corresponding to skin stress resultants of 0.026 to 2.7 lb/in.

Buckles were detected visually and usually were accompanied by a sudden pressure change noticeable on the differential pressure indicator. Since this sudden change was not always in evidence, the buckling pressures have been taken to be the highest differential pressure which could be attained under essentially static loading conditions. Pressures were recorded manually, and the data were supplemented with photographs.

Results

Buckling test sequences for the 30-inch-diameter specimen under a low and a high inflation pressure are shown in figures 7 and 8, respectively. Similar buckling test sequences for the 12.5-foot-diameter specimen are shown in figures 9 and 10. Note the marked initial imperfections at zero differential pressure for the low initial inflation pressures as compared with the relatively undeformed surfaces for the high initial inflation pressures.

The results of buckling tests of the two spheres are summarized in table I. The first column under the heading "Prestress" gives the differential pressure to which the specimen was initially inflated. The second column gives the stress resultant in the skin developed by this initial pressure. In the next column is listed the excess buoyant force (12.5-foot-diameter sphere only) or the downward force exerted by the support when buckling occurred. The columns under the heading "Buckling" give the pressure differential at buckling in inches of water, in pounds per square inch, and finally as a ratio of measured buckling pressure differential to a theoretical buckling pressure calculated from classical linear theory. The theoretical buckling pressure differential for the laminated shell wall was obtained by use of the following equation:

$$\Delta p_{cl} = \left(\frac{2}{r}\right)^2 \sqrt{DK}$$

The values of D and K are calculated from the maximum measured wall thicknesses and the highest values of E_a and E_f as given in appendix C and are for a wrinkle-free wall.

The first column under the heading "Echo A-12" gives the classical buckling pressure differential calculated from the nominal wall thicknesses (appendix C). If the test specimens were fabricated of the same material as the full-scale satellite, then according to the classical theory the ratio of the buckling pressure of the Echo A-12 satellite to the buckling pressure of a smaller sphere would simply vary inversely as the square of the ratio of the radii. However, thickness measurements made on the test specimens indicated thicknesses which differed significantly from the nominal wall thicknesses for the full-scale satellite. Thus, in order to obtain conservative estimates of the buckling strength of the full-scale satellite, the following equation was used:

$$(\Delta p)_{A12} = \left(\frac{\Delta p}{\Delta p_{cl}}\right)_m \left(\Delta p_{cl}\right)_{A12} \qquad (D1)$$

where $(\Delta p)_{A12}$ is the estimated buckling pressure differential for the full-scale satellite, $\left(\frac{\Delta p}{\Delta p_{cl}}\right)_m$ is a ratio of the measured buckling pressure differential for a test specimen to the classical buckling pressure differential computed from thickness measurements made on the specimen, and $\left(\Delta p_{cl}\right)_{A12}$ is the classical buckling pressure for the full-scale sphere computed from nominal thicknesses, which are smaller than the thicknesses measured on the test specimens. The second column under this heading gives the conservative estimates of $(\Delta p)_{A12}$ obtained from equation (D1).

The final column under the heading "Echo A-12" gives a ratio of the estimated buckling pressure differential of the full-scale satellite to the solar pressure obtained from figure 1. This ratio may be considered to be a safety factor for buckling of the Echo A-12 satellite due to solar pressure. The lowest safety factor is 142, which corresponds to an estimated buckling pressure differential of 1.85×10^{-7} psi. This value corresponds to the dynamic pressure on a satellite in a circular orbit at an altitude of about 215 international nautical miles (see fig. 1). Since the data of figure 1 were obtained during a period of intense solar flare activity, in which the earth's atmosphere is known to expand, 215 international nautical miles should be a conservative estimate of the minimum altitude at which the Echo A-12 satellite can withstand the dynamic pressure.

The lowest safety factor was obtained from experience with the 30-inch-diameter sphere. Considerably higher safety factors were obtained from experience with the 12.5-foot-diameter sphere and ranged as high as 582.

The data of table I are shown in figure 5, where for both test specimens the ratios $\left(\frac{\Delta p}{\Delta p_{cl}}\right)_m$ and $\frac{(\Delta p)_{A12}}{(\Delta p)_{sol}}$ are plotted as functions of the skin stress resultant due to initial inflation N_o. Note that as initial skin stress resultant increases, the buckling pressure first increases and then decreases. For the 30-inch-diameter sphere $\left(\frac{\Delta p}{\Delta p_{cl}}\right)_m$ varies from 0.044 to 0.110, and for the 12.5-foot-diameter sphere the quantity varies from 0.122 to 0.182. At the highest values of initial skin stress resultant some permanent deformation in the gores of laminate material was observed. A simple analysis indicated that at these values of skin stress resultant the aluminum faces had very likely yielded significantly. Since the sphere wall was of double thickness at the splices, the material tended to stretch mostly in the gores. This permanent deformation in the gores may have acted as an imperfection to induce buckling at a lower pressure differential.

Correction to Experimental Data

Because of the difference in density between the gas inside the specimens and the surrounding atmosphere, the pressure differential across the walls of the specimens varied with vertical location. This variation in differential pressure was not the same for the two specimens. Also, the possibility was investigated that corrections to the data might be necessary due to any difference in vertical location of the micromanometer and the buckles in the specimens.

When buckling occurred, the largest pressure differential was at the bottom of the sphere. In addition, any excess buoyant force was balanced by a downward concentrated force at the stem. As a result of these factors, buckles almost invariably appeared in the lower hemisphere. The only exceptions occurred in tests on the 30-inch-diameter sphere in which the buckles shifted to the top of the sphere for the three highest values of initial inflation pressure.

To determine the necessary corrections to the experimental data, a simple analysis has been made on the assumption of linear variations of internal and external pressure with height. This assumption is quite appropriate for the vertical distances involved in these tests. The analysis indicated that the most conservative corrections would be obtained when the assumption was made that the pressurization gas contained just enough helium to counteract the weight of the specimen; therefore, all corrections to the experimental data have been made subject to this assumption.

The micromanometer was set up to measure the difference in pressure between two points, one inside and one outside the sphere. If the bottom of the sphere is chosen as a reference point, the following expression for the corrected buckling pressure differential is obtained:

$$\Delta p = (\Delta p)_{man} + (\rho - \rho_i)(b - x) \qquad (D2)$$

where

$(\Delta p)_{man}$ differential pressure reading at micromanometer, in. H_2O

ρ weight density of sea-level standard atmosphere, in. H_2O/in.

ρ_i weight density of pressurization gas ($<\rho$), in. H_2O/in.

b vertical distance from bottom of sphere to point on micromanometer at which differential pressure was measured, in.

x vertical distance from bottom of sphere to center of buckle, in.

Equation (D2), along with the appropriate values for the parameters, has been used to make all the necessary corrections.

30-inch-diameter specimen.- In practically all the tests with the 30-inch-diameter sphere, equation (D2) yielded an experimental buckling pressure higher than was indicated, since the buckles usually occurred at points below the micromanometer. However, for the three highest values of prestress, the buckles shifted to a point near the top of the sphere and slightly above the micromanometer. This shift required a small downward correction to the measured buckling pressure. Conservative corrections to the experimental data were as large as 39 percent of the indicated values at the smaller values of buckling pressure.

12.5-foot-diameter specimen.- For the 12.5-foot-diameter specimen the differential pressure indicator was located at approximately the height at which the buckles appeared; therefore, no significant correction to the measured buckling pressures appeared necessary. Corrections to the measured initial inflation pressures were required, however, since the micromanometer used for these pressure measurements was located above the buckling region. Even so, these corrections are insignificant for all but the lowest initial inflation pressures. The atmospheric pressure change over the vertical distance from the buckling region to the micromanometer was computed as 0.001 inch of water. This correction has been made to the lower initial inflation pressures.

Accuracy of Results

Some remarks concerning the accuracy of the uncorrected and corrected experimental data are perhaps in order. The two most important units of testing apparatus were the micromanometer and the highly sensitive differential pressure indicator. The micromanometer has a least count of 0.0001 inch of water and, from available information, is quite accurate to this least count. Generally, the reading error is probably on the order of ±0.002 inch of water.

The differential pressure indicator used in the tests with the 12.5-foot-diameter specimen measures the difference in pressure between two reservoirs by measuring the rate of flow through a tube from one reservoir to the other. According to information supplied by the manufacturer, this instrument is accurate to within 6 or 7 percent of the measured pressure in the range covered in these tests.

Corrections to the experimental data based on the assumption of a linear variation of atmospheric pressure with height should contain no significant error. The conservative assumption that each sphere contained only enough helium to support it is obviously quite reasonable for the 12.5-foot-diameter specimen; no measurements of the buoyant force were made during the tests on the 30-inch-diameter specimen. However, it is believed that no further appreciable upward correction due to a surplus of helium in the pressurization gas is warranted.

In view of the corrections made and the possibility of errors in pressure measurement, it is believed that the true buckling pressures exceed the reported values, particularly for the 30-inch-diameter specimen.

REFERENCES

1. Anon.: Mylar - Physical, Electrical, and Chemical Properties. Tech. Rep. TR-1, E. I. Du Pont de Nemours & Co., Inc.

2. Minzner, R. A., Champion, K. S. W., and Pond, H. L.: The ARDC Model Atmosphere, 1959. Air Force Surveys in Geophysics No. 115 (AFCRC-TR-59-267), Air Force Cambridge Res. Center, Aug. 1959.

3. Clemmons, Dewey L., Jr.: The Echo I Inflation System. NASA TN D-2194, 1964.

4. Aerospace Group: Final Report - Space Structure Rigidization. P61-13 (Contract NAS1-847), Hughes Aircraft Co., Sept. 8, 1961.

5. Weinitschke, Hubertus J.: Asymmetric Buckling of Clamped Shallow Spherical Shells. Collected Papers on Instability of Shell Structures - 1962. NASA TN D-1510, 1962, pp. 481-490.

6. Tsien, Hsue-Shen: A Theory for the Buckling of Thin Shells. Jour. Aero. Sci., vol. 9, no. 10, Aug. 1942, pp. 373-384.

7. Kaplan, A., and Fung, Y. C.: A Nonlinear Theory of Bending and Buckling of Thin Elastic Shallow Spherical Shells. NACA TN 3212, 1954.

8. Klöppel, Kurt, and Jungbluth, Otto: Beitrag zum Durchschlagproblem dünnwandiger Kugelschalen. Der Stahlbau, Jahrg. 22, Heft 6, June 1953, pp. 121-130.

9. Goerner, Erich: Buckling Characteristics of Spherical or Spherically-Dished Shells. Rep. 1R9, Army Ballistic Missile Agency (Huntsville, Ala.), Feb. 6, 1956.

10. Homewood, R. H., Brine, A. C., and Johnson, Aldie E., Jr.: Experimental Investigation of the Buckling Instability of Monocoque Shells. Exp. Mech., vol. 1, no. 3, Mar. 1961, pp. 88-96.

11. Fung, Y. C., and Sechler, E. E.: Instability of Thin Elastic Shells. Structural Mechanics, J. Norman Goodier and Nicholas J. Hoff, eds., Pergamon Press (New York), 1960, pp. 115-168.

12. Reynolds, Thomas E.: A Survey of Research on the Stability of Hydrostatically-Loaded Shell Structures Conducted at the David Taylor Model Basin. Collected Papers on Instability of Shell Structures - 1962. NASA TN D-1510, 1962, pp. 551-560.

13. Timoshenko, S., and Woinowsky-Krieger, S.: Theory of Plates and Shells. Second ed., McGraw-Hill Book Co., Inc., 1959.

14. Timoshenko, Stephen P., and Gere, James M.: Theory of Elastic Stability. Second ed., McGraw-Hill Book Co., Inc., 1961.

15. Jahnke, Eugene, and Emde, Fritz: Tables of Functions. Fourth ed., Dover Publ., 1945.

16. Seide, P., Weingarten, V. I., and Morgan, E. J.: Final Report on the Development of Design Criteria for Elastic Stability of Thin Shell Structures. STL/TR-60-0000-19425 (AFBMD/TR-61-7), Space Tech. Labs., Inc., Dec. 31, 1960.

17. Bickley, W. G.: The Heavy Elastica. Phil. Mag., vol. 17, Mar. 1934, pp. 603-622.

TABLE I.- RESULTS OF BUCKLING TESTS ON SPHERES FABRICATED OF ECHO A-12 LAMINATE

Test	Prestress		Buoyant force, lb	Buckling			ECHO A-12		
	Δp, in. H_2O	Stress resultant, lb/in.		Δp, in. H_2O	Δp, psi	$\left(\frac{\Delta p}{\Delta p_{cl}}\right)_m$	$(\Delta p_{cl})_{A12}$, psi (nominal)	$(\Delta p)_{A12}$, psi	$\frac{(\Delta p)_{A12}}{(\Delta p)_{sol}}$
(a) 30-inch-diameter sphere									
1	-0.034	0.0092		0.047	1.69×10^{-3}	0.065	52.0×10^{-7}	2.70×10^{-7}	208
2	-.109	.029		.032	1.15	.044		1.85	142
3	-.259	.070		.037	1.33	.0514		2.14	164
4	-.509	.138		.040	1.44	.0556		2.31	178
5	-.759	.205		.046	1.66	.0641		2.66	205
6	-1.0	.27		.048	1.73	.0668		2.78	214
7	-1.5	.41		.051	1.84	.0711		2.96	228
8	-2.0	.54		.064	2.30	.0888		3.70	284
9	-2.5	.68		.061	2.20	.085		3.54	272
10	-3.0	.81		.072	2.59	.100		4.16	320
11	-4.0	1.1		.079	2.84	.110		4.58	352
12	-6.0	1.6		.049	1.76	.068		2.83	218
13	-8.0	2.2		.057	2.05	.0792		3.30	254
14	-10.0	2.7		.048	1.73	.0668	↓	2.78	214
(b) 12.5-foot-diameter sphere									
1	-0.019	0.026	0.10	0.0035	1.26×10^{-3}	0.122	52.0×10^{-7}	5.09×10^{-7}	390
2	-.049	.066	.05	.0035	1.26	.122		5.09	390
3	-.074	.10	.10	.0037	1.34	.129		5.38	413
4	-.10	.14	.20	.0037	1.34	.129		5.38	413
5	-.20	.27	.10	.0040	1.45	.140		5.82	448
6	-.30	.41	.15	.0044	1.59	.154		6.40	493
7	-.40	.54	.10	.0045	1.63	.157		6.53	502
8	-.50	.68	.10	.0045	1.63	.157		6.53	502
9	-.75	1.0	.05	.0050	1.81	.175		7.30	560
10	-1.0	1.4	.10	.0052	1.88	.182		7.58	582
11	-1.5	2.0	.10	.0045	1.66	.157		6.53	502
12	-2.0	2.7	.10	.0047	1.70	.164	↓	6.82	525

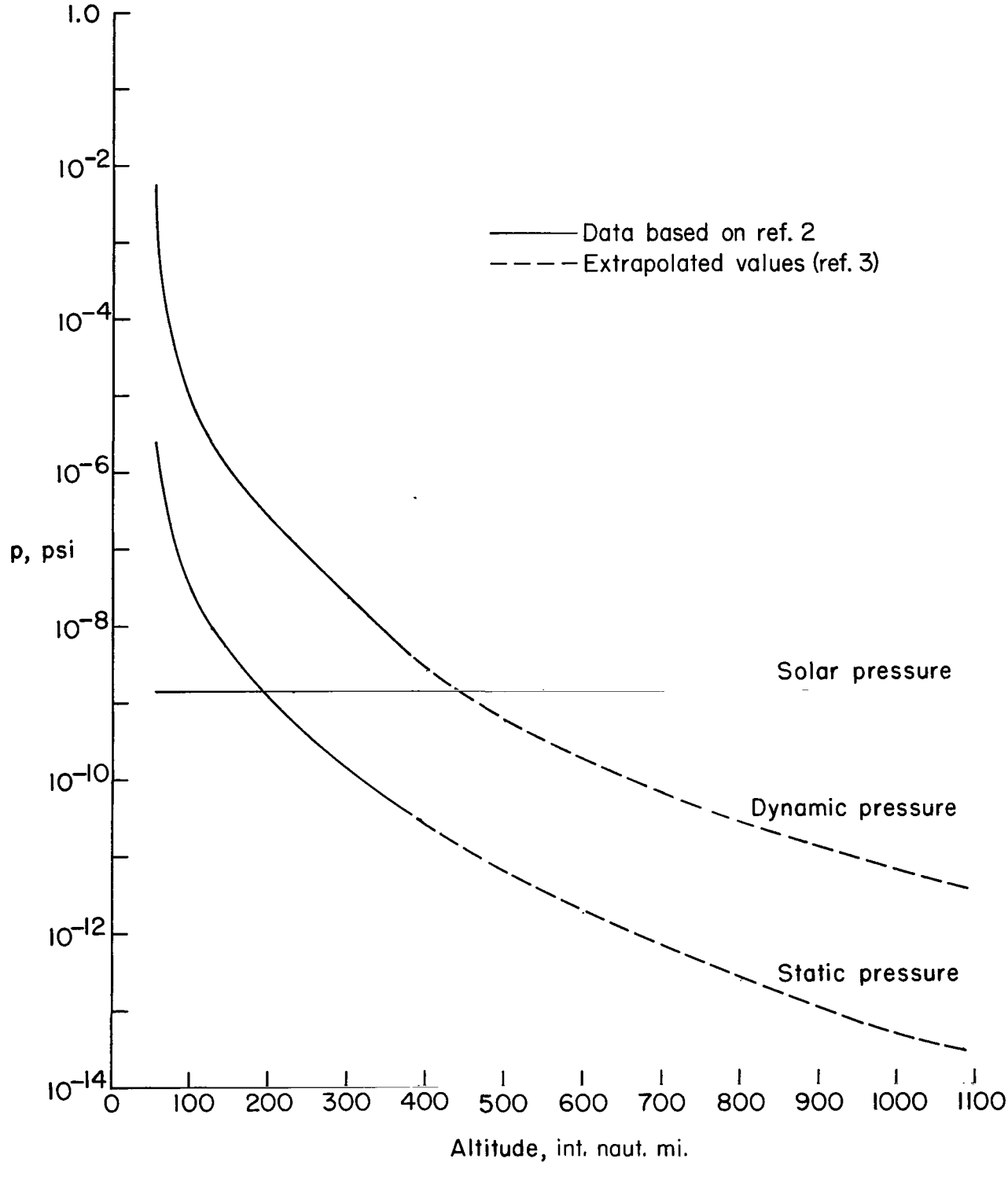

Figure 1.- Solar pressure and dynamic pressure for a circular orbit as a function of altitude.

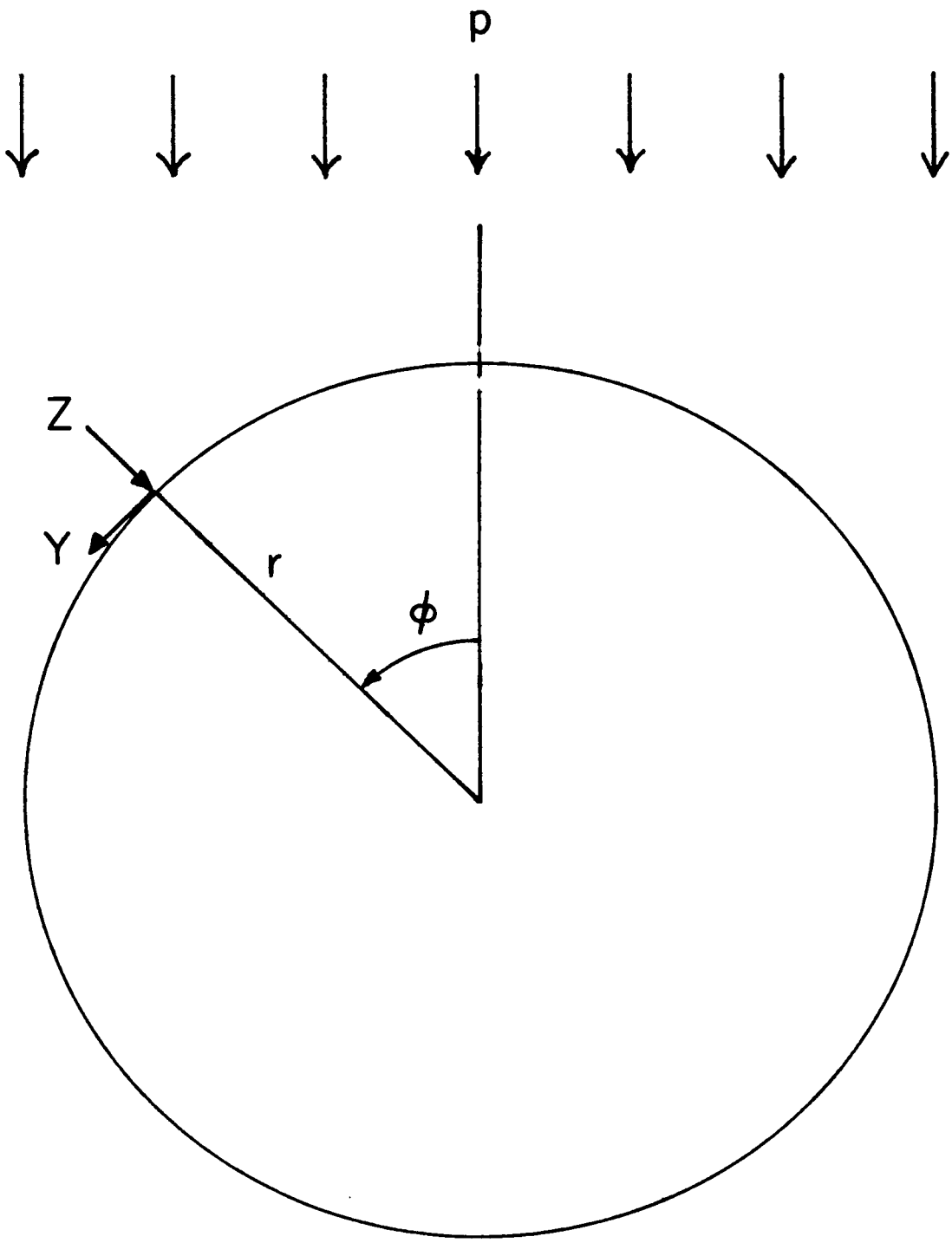

Figure 2.- Coordinate system.

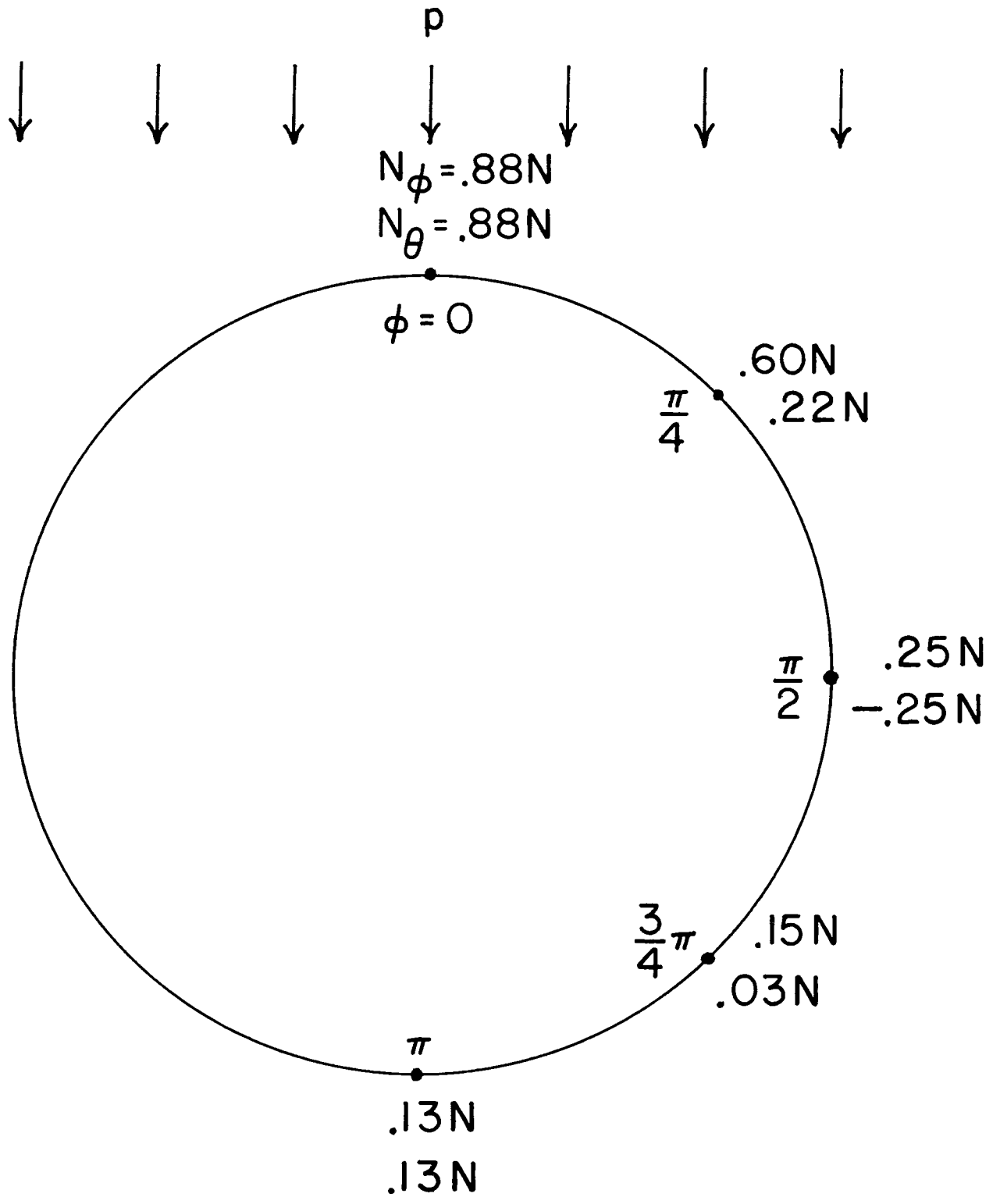

Figure 3.- Distribution of stress resultants due to solar or dynamic pressure. $N = -\frac{pr}{2}$.

Figure 4.- Folded 12.5-foot-diameter sphere. L-64-3018

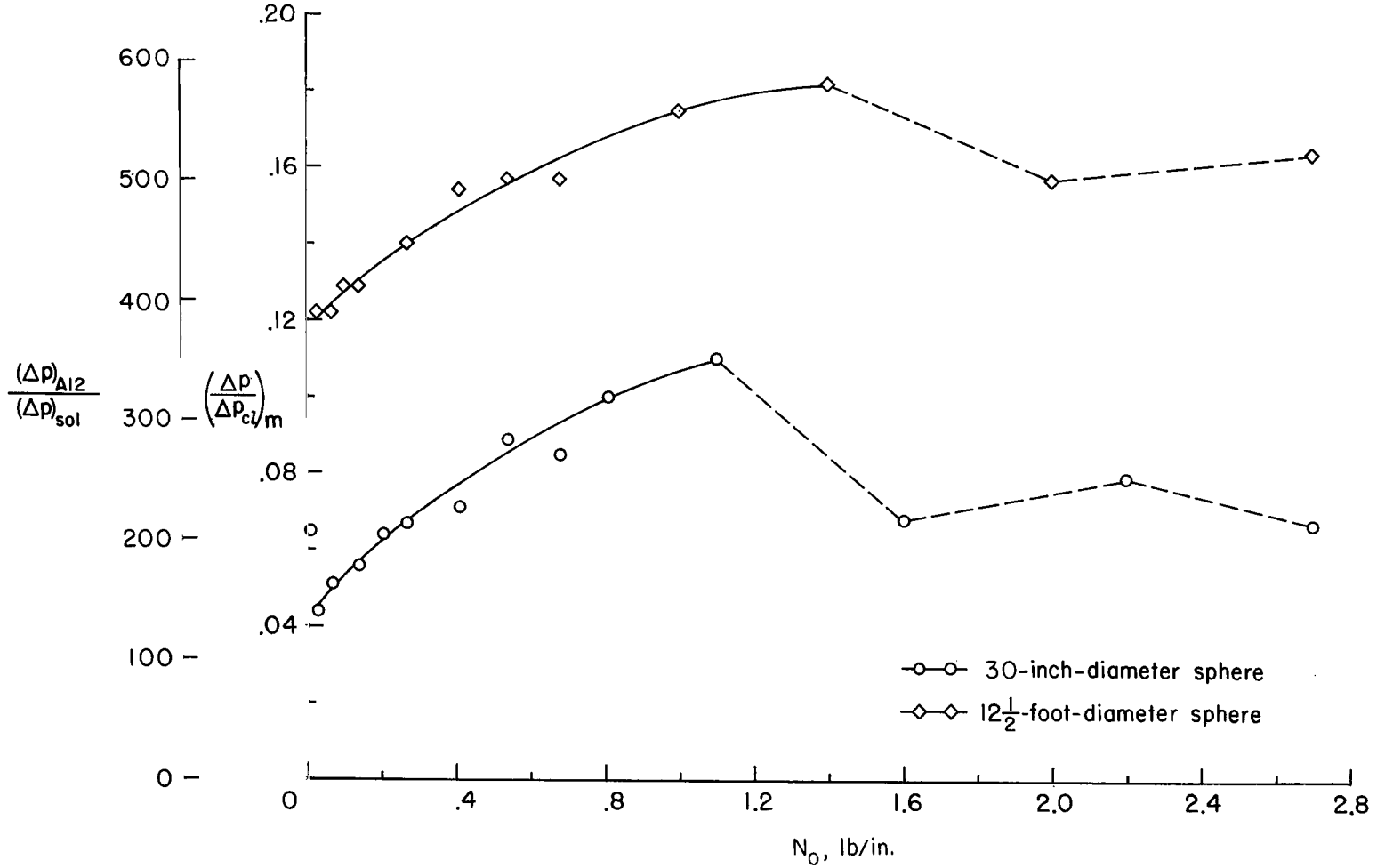

Figure 5.- Results of buckling tests on complete spheres and estimated buckling pressures of full-scale satellite (dashed portion of curves indicates probable yielding of aluminum faces under prestress).

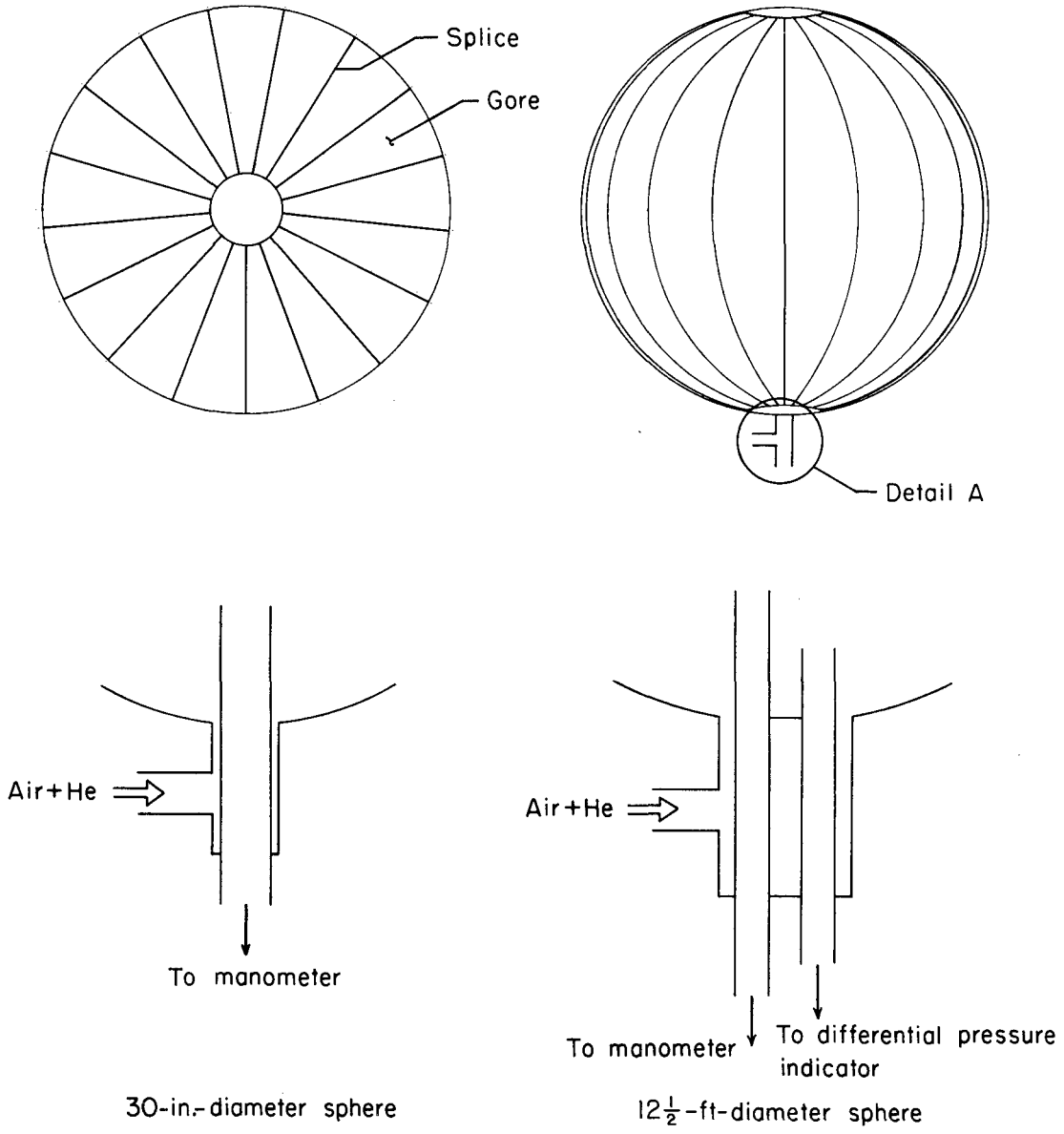

(a) Sketch of specimen.

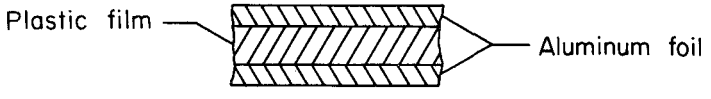

(b) Section of specimen wall.

Figure 6.- Schematic of specimens and pressurization attachments.

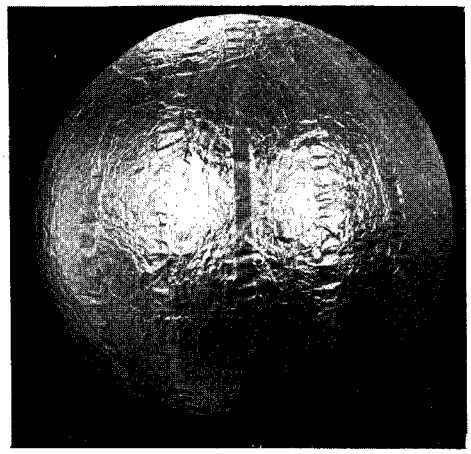

(a) Δp_o = -0.509 in. H_2O.

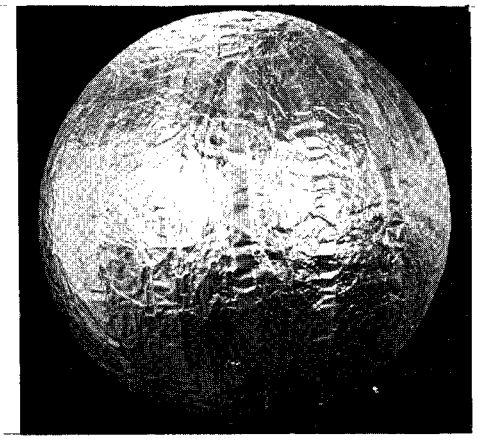

(b) Δp = 0.

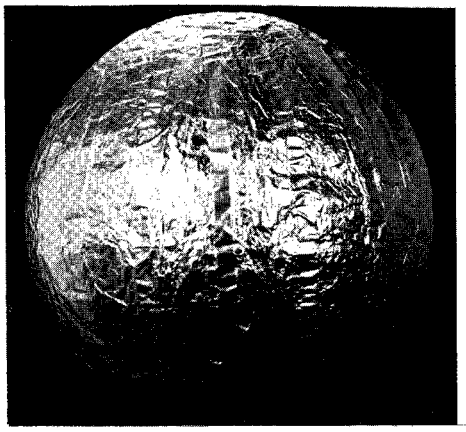

(c) After buckling (at buckling, Δp = 0.040 in. H_2O). L-64-3019

Figure 7.- Buckling test sequence for 30-inch-diameter sphere. Low inflation pressure.

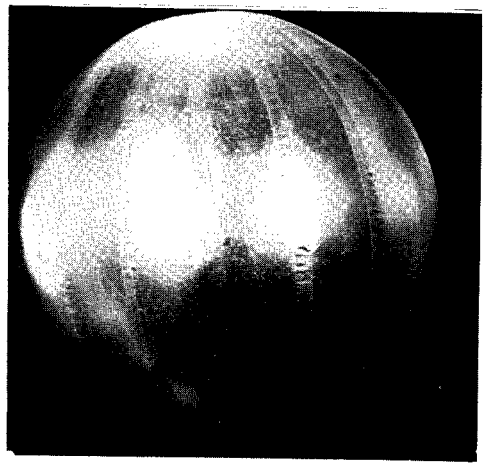

(a) Δp_o = -10 in. H_2O.

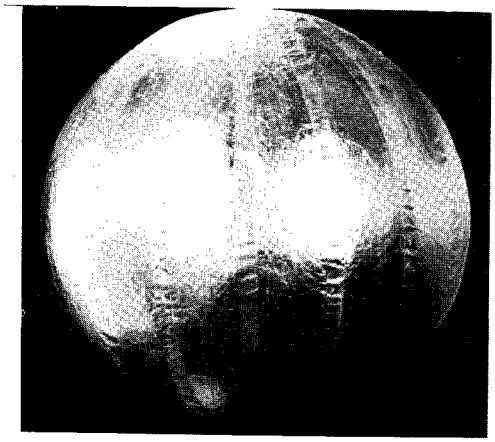

(b) Δp = 0.

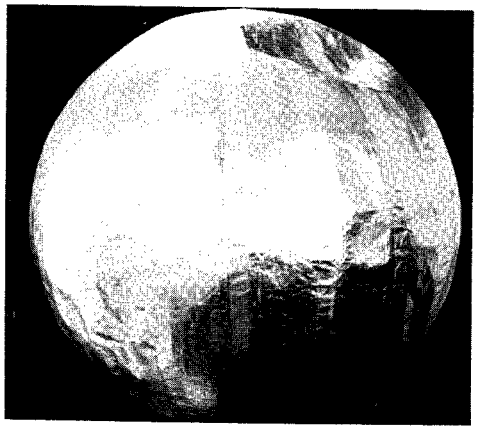

(c) After buckling (at buckling, Δp = 0.048 in. H_2O). L-64-3020

Figure 8.- Buckling test sequence for 30-inch-diameter sphere. High inflation pressure.

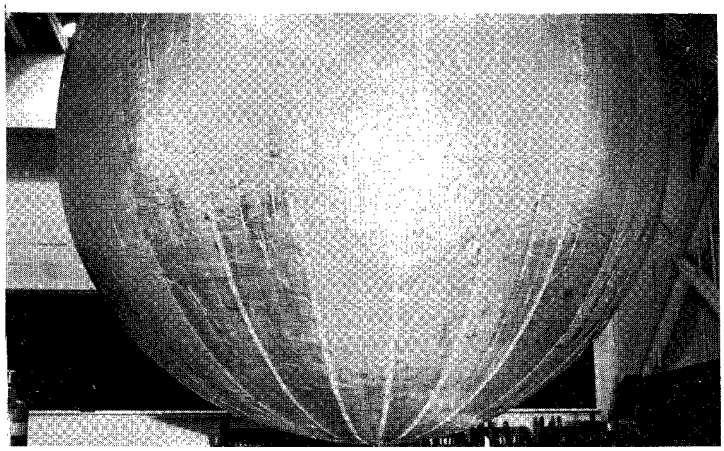

(a) Δp_o = -0.074 in. H_2O.

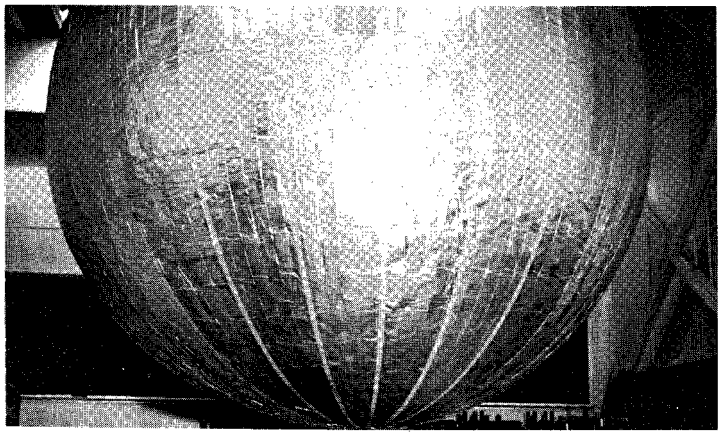

(b) Δp = 0.

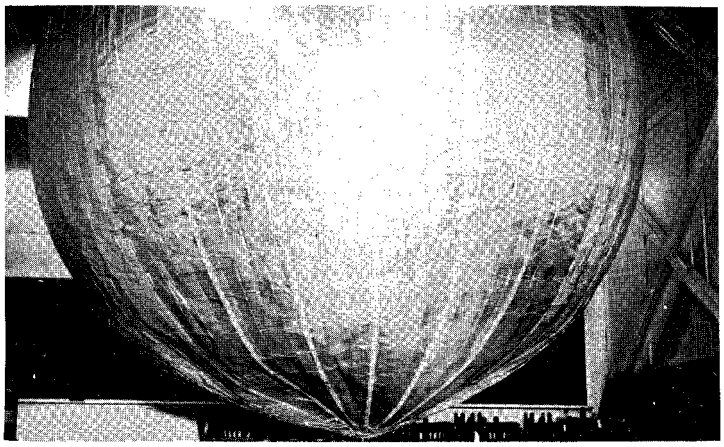

(c) After buckling (at buckling, Δp = 0.0037 in. H_2O). L-64-3021

Figure 9.- Buckling test sequence for 12.5-foot-diameter sphere. Low inflation pressure.

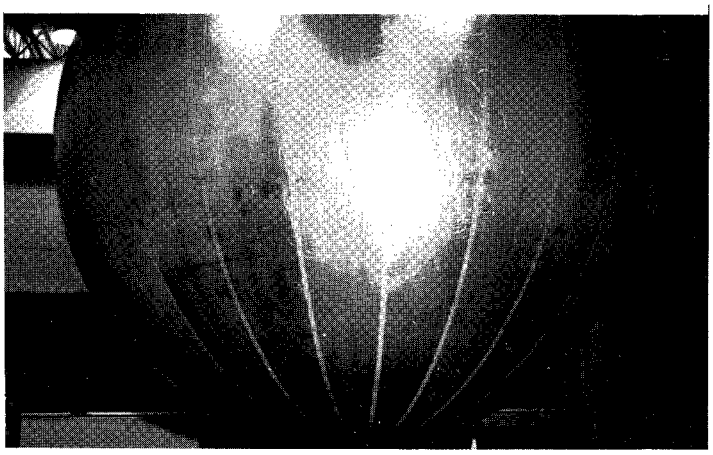

(a) Δp_o = -0.50 in. H_2O.

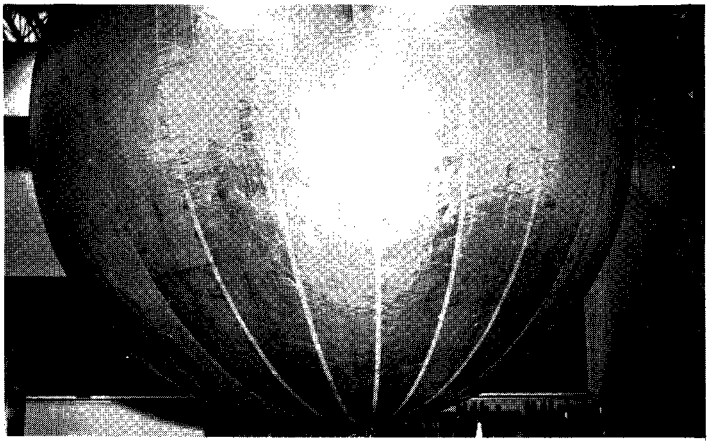

(b) Δp = 0.

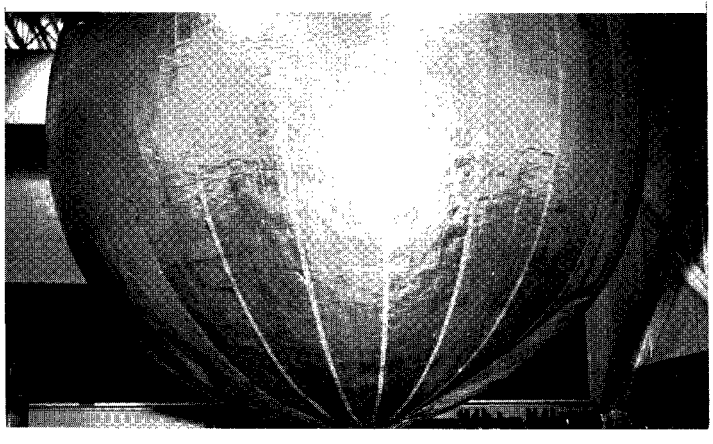

(c) After buckling (at buckling, Δp = 0.0045 in. H_2O). L-64-3022

Figure 10.- Buckling test sequence for 12.5-foot-diameter sphere. High inflation pressure.

2/12/21
B

"The aeronautical and space activities of the United States shall be conducted so as to contribute . . . to the expansion of human knowledge of phenomena in the atmosphere and space. The Administration shall provide for the widest practicable and appropriate dissemination of information concerning its activities and the results thereof."

—NATIONAL AERONAUTICS AND SPACE ACT OF 1958

NASA SCIENTIFIC AND TECHNICAL PUBLICATIONS

TECHNICAL REPORTS: Scientific and technical information considered important, complete, and a lasting contribution to existing knowledge.

TECHNICAL NOTES: Information less broad in scope but nevertheless of importance as a contribution to existing knowledge.

TECHNICAL MEMORANDUMS: Information receiving limited distribution because of preliminary data, security classification, or other reasons.

CONTRACTOR REPORTS: Technical information generated in connection with a NASA contract or grant and released under NASA auspices.

TECHNICAL TRANSLATIONS: Information published in a foreign language considered to merit NASA distribution in English.

TECHNICAL REPRINTS: Information derived from NASA activities and initially published in the form of journal articles.

SPECIAL PUBLICATIONS: Information derived from or of value to NASA activities but not necessarily reporting the results of individual NASA-programmed scientific efforts. Publications include conference proceedings, monographs, data compilations, handbooks, sourcebooks, and special bibliographies.

Details on the availability of these publications may be obtained from:

SCIENTIFIC AND TECHNICAL INFORMATION DIVISION

NATIONAL AERONAUTICS AND SPACE ADMINISTRATION

Washington, D.C. 20546